Distinct Effects of Humic Acid on Transport and Retention of TiO2 Rutile Nanoparticles in Saturated Sand Columns

ARTICLE *in* ENVIRONMENTAL SCIENCE & TECHNOLOGY · JUNE 2012

Impact Factor: 5.33 · DOI: 10.1021/es204010g · Source: PubMed

3 AUTHORS:

Gexin Chen
United States Environmental Protection Agency
17 PUBLICATIONS **393** CITATIONS
SEE PROFILE

Xuyang Liu
United States Environmental Protection Agency
12 PUBLICATIONS **405** CITATIONS
SEE PROFILE

Chunming Su
United States Environmental Protection Agency
53 PUBLICATIONS **2,267** CITATIONS
SEE PROFILE

Environmental Science & Technology

Article

pubs.acs.org/est

Distinct Effects of Humic Acid on Transport and Retention of TiO_2 Rutile Nanoparticles in Saturated Sand Columns

Gexin Chen,[†,*] Xuyang Liu,[†] and Chunming Su[‡]

[†]National Research Council Resident Research Associate and [‡]Ground Water and Ecosystems Restoration Division, National Risk Management Research Laboratory, Office of Research and Development, U.S. Environmental Protection Agency, 919 Kerr Research Drive, Ada, Oklahoma 74820, United States

Supporting Information

ABSTRACT: The distinct effects of humic acid (HA, 0−10 mg L^{-1}) on the transport of titanium dioxide (rutile) nanoparticles ($nTiO_2$) through saturated sand columns were observed under conditions of environmental relevance (ionic strength 3−200 mM NaCl, pH 5.7 and 9.0). Specifically, the transport of $nTiO_2$ was dramatically enhanced in the presence of HA at pH 5.7, even at a low HA concentration of 1 mg L^{-1}. The mobility of $nTiO_2$ was further increased with greater concentrations of HA. In contrast, this enhancement of the $nTiO_2$ transportability due to the presence of HA was limited at pH 9.0 because of the negligible adsorption of HA onto $nTiO_2$, regardless of the concentrations of HA examined in this study. The distinct effects can be explained by the adsorption behaviors of HA to $nTiO_2$ and sand surfaces and the resulting interactions between $nTiO_2$ and sand surfaces under different conditions, which resulted in a large variation of the $nTiO_2$ transport and deposition behaviors at various conditions. In addition, theoretical interaction energy calculations and additional elution experiments indicate that the secondary energy minimum played an important role in controlling the $nTiO_2$ transport and deposition in porous media observed in this study. Moreover, the interaction energy calculations suggest that at pH 5.7, HA affected $nTiO_2$ transport by increasing the negative surface charge of $nTiO_2$ at low HA adsorption densities; whereas, combinations of increased electrostatic and steric interactions due to the presence of HA were the main mechanisms of enhanced transportability of $nTiO_2$ at high HA adsorption densities. Overall, results from this study suggest that natural organic matter and solution pH are likely key factors that govern the stability and mobility of $nTiO_2$ in the natural aquatic environment.

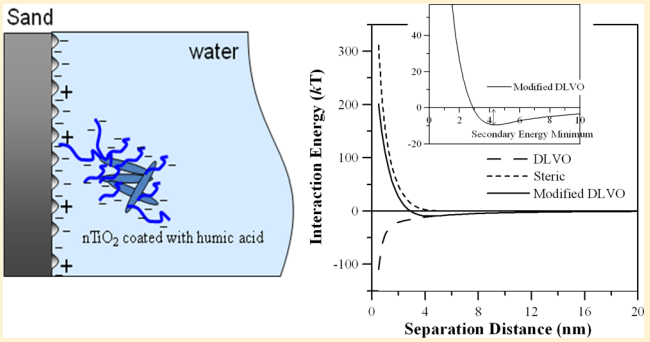

1. INTRODUCTION

Nanoscale titanium dioxide ($nTiO_2$), one of the most extensively manufactured metal oxide nanomaterials, has been increasingly used in a variety of applications and commercial products, including photocatalysts, sunscreens, coatings, paints, and pigments due to its performance enhancement capability.[1,2] Given its expansive production and use,[3] some of the $nTiO_2$ is being released into the natural aquatic environment.[4−6] However, accumulated evidence has shown the adverse exposure effects of engineered $nTiO_2$ on aquatic organisms including microbes, algae, invertebrates, and fish.[7] Furthermore, recent studies suggest that $nTiO_2$ may facilitate the transport of coexisting pollutants and considerably augment their ecotoxicity by adsorption of the environmental contaminants onto the $nTiO_2$ and thereafter internalization of the $nTiO_2$ by microorganisms, which makes it necessary to examine both its direct impacts and possible indirect effects of interactions with other environmental contaminants in terms of assessing the environmental risk and ecological implications of the $nTiO_2$ exposure.[8] Indeed, TiO_2 has widely been used as a model mineral for organic and inorganic pollutant adsorption studies due to its well-characterized surface properties and its ability to readily bind pollutants including the highly toxic marine antifouling compound tributyltin, radionuclides, and arsenic to its surface under conditions of environmental relevance.[8−10] Hence, in order to reasonably evaluate such unintended environmental consequences of the release and accumulation of engineered $nTiO_2$ in the environment, thorough examination of the persistence and mobility of the $nTiO_2$ at environmentally relevant conditions is a critical component of risk assessment, as its bioavailability and toxicity will inevitably be governed by its fate and transport in the environment.[11]

A number of transport and deposition studies of engineered $nTiO_2$ have been conducted utilizing well-controlled porous media packed in columns.[12−20] These studies have offered great insights into the transport and deposition behavior of $nTiO_2$ in saturated porous media under various physicochemical and/or

Received: November 10, 2011
Revised: May 29, 2012
Accepted: June 4, 2012
Published: June 4, 2012

geochemical conditions of environmental interest and have important implications for the fate and transport of $nTiO_2$ in natural systems. In general, limited transport of $nTiO_2$ without surface modification was often reported in clean porous media when the pH of $nTiO_2$ suspensions approached the point of zero charge (pH_{pzc}) of $nTiO_2$ particles, which facilitated $nTiO_2$ aggregation.[14−18,20] In these studies, the concurrence of aggregation and deposition of $nTiO_2$ in the column was often observed. As a result, the aggregation process increased $nTiO_2$ retention.[16,17,20] On the contrary, the stability and mobility of $nTiO_2$ were markedly enhanced when the pH of suspensions moved far from its pH_{pzc}, especially at alkaline conditions.[2,16] These observations suggest that electrostatic interactions between surfaces (i.e., $nTiO_2$−$nTiO_2$ and $nTiO_2$−sand), to a large extent, dominate the transport and deposition behavior of $nTiO_2$ in porous media, which is consistent with the physicochemical properties of TiO_2 surface. It is known that TiO_2 has limited surface charge density when the aqueous solution pH approaches its pH_{pzc}; whereas, its surface readily develops a considerable negative charge density at alkaline conditions through the deprotonation of its surface hydroxyl groups.[21,22] However, the majority of these studies overlooked the impact of a critical component—natural organic matter (NOM) on the fate and transport of $nTiO_2$.[23]

NOM ubiquitously exists in natural waters. Adsorption of NOM to nanoparticle (NP) surface significantly alters NP physicochemical characteristics, and, as a result, affects NP stability and mobility in aquatic environments. Previous colloidal particle filtration studies demonstrated that the presence of NOM can significantly influence, sometimes dominate the aqueous stability and mobility of engineered NPs including nano zerovalent iron,[24] fullerenes,[25,26] carbon nanotubes,[27] and zinc oxide NPs, [28] and natural colloids (e.g., clay, hematite, and surrogate particles).[29−32] In these studies, the stability and mobility of the engineered NPs were considerably enhanced as the adsorbed NOM effectively increased electrostatic and/or steric repulsive interactions between surfaces. Similar impact of NOM was reported for $nTiO_2$ with a concentration of 60 mg L^{-1} humic acid (HA) present in $nTiO_2$ suspensions, which was the sole study that briefly examined the impact of NOM on $nTiO_2$ transport.[19]

The main objective of this work was to gain more insight into the effects of NOM on the transport and deposition of $nTiO_2$ in saturated porous media under conditions of subsurface environment relevance. Systematic column experiments with $nTiO_2$, supplemented with necessary characterization tests, were performed. Suwannee River humic acid (SRHA) was used to represent the major component of NOM in subsurface environments. The initial deposition kinetics of $nTiO_2$ under a wide range of solution conditions was determined on the basis of column experiments. Subsequently, the effects of SRHA on the interactions of $nTiO_2$ with sand surfaces and, as a result, on the transport and deposition behavior of $nTiO_2$ in porous media were elucidated and discussed.

2. MATERIALS AND METHODS

2.1. Preparation of $nTiO_2$ Suspensions and Solution Chemistry. TiO_2 nanoparticles (NPs) were obtained from Nanostructured & Amorphous Materials, Inc. (rutile, stock no. 5480MR, 98+%; Houston, TX) with a nominal size of 10 × 40 nm. The specific surface area of the NPs was measured to be 155.11 ± 1.12 m^2 g^{-1} (n = 2) in a multipoint BET mode using a NOVA Surface Area Analyzer (Quantachrome Instruments, Boynton Beach, FL). The NPs have an isoelectric point (IEP) of 4.4 as determined in our previous study and the low IEP is most likely caused by the impurity elements such as silicon and phosphorus residing on the NP surface during the NPs manufacturing process.[33] Immediately prior to each experiment, an aqueous suspension containing a final $nTiO_2$ concentration of 20 mg L^{-1} and the desired solution chemistry was prepared. A wide range of environmentally relevant background solution chemistries was examined in transport experiments: ionic strength (IS) 3−200 mM (sodium chloride, NaCl), SRHA concentration 0−10 mg L^{-1} at pH 5.7 and 9.0. The SRHA supplied by the International Humic Substances Society (St. Paul, MN) was used as a model material for humic substances. It has an estimated average molecular weight of 1066 Da and contains about 4.9 mmol g^{-1} carboxyl groups and 2.9 mmol g^{-1} phenol groups.[34] To achieve a constant pH of 9.0 ± 0.1 in $nTiO_2$ suspensions, background solutions were buffered with 0.4 mM $NaHCO_3$ and 0.1 mM Na_2CO_3. Detailed methods and techniques of $nTiO_2$ suspension preparation and characterization including the electrophoretic mobility, particle size distribution, and the stability of the prepared $nTiO_2$ suspensions are provided in the Supporting Information (SI).

2.2. Adsorption of SRHA to $nTiO_2$. Adsorption studies were conducted to determine the adsorbed amount of SRHA to $nTiO_2$ at conditions identical to those used in transport experiments (~31 min for SRHA adsorbing to $nTiO_2$ before centrifugation). Immediately after the completion of the $nTiO_2$ suspension preparation, 30 mL of the suspension was added into a clean centrifuge tube and suspended $nTiO_2$ particles were pelleted by sequential centrifugation (Sorvall RC5C centrifuge, Dupont Instruments). The SRHA concentration in supernatant was determined using a spectrophotometer (UV-3101PC, Shimadzu Corporation, Columbia, MD) at 254 nm.[31,35] The adsorbed SRHA was then determined by the difference between the initial and final SRHA concentrations in the aqueous phase. The results were reported as mg SRHA/m^2 $nTiO_2$ for each condition. The complete procedure is given in the SI.

2.3. Column Experiments. Glass chromatography columns (2.5 cm in diameter and 10 cm in length) were wet-packed uniformly with clean sand having an average sand diameter of approximately 275 μm. The resulting porosity of the porous media was gravimetrically determined to be ca. 0.37. Once packed, the column was flushed with deionized (DI) water and then pre-equilibrated with a 400-mL solution with desired background IS, SRHA concentration, and pH overnight. This pre-equilibration procedure was essential in producing consistent transport results, similar to the observation reported by Amirbahman and Olson.[31] The Darcy velocity was maintained at 5.1 × 10^{-3} cm s^{-1} for all experiments. A pulse of the $nTiO_2$ suspension (20 mg L^{-1}) with the same background electrolyte compositions was then introduced into the column for 4 PVs, followed by a NP-free background electrolyte solution (ca. 4 PVs) injection. Column effluent samples were collected in 20-mL liquid scintillation vials using a fraction collector (Retriever 500, Teledyne Isco, Inc., Lincoln, NE). The influent (C_0) and effluent concentrations (C) of NPs were determined with a spectrophotometer at 286 nm. Following completion of each transport experiment, the spatial distribution of the $nTiO_2$ retained in the column was also determined. Additional information about the column experiments is provided in the SI.

3. RESULTS AND DISCUSSION

3.1. SRHA Adsorption to $nTiO_2$. SRHA adsorption to $nTiO_2$ (20 mg L^{-1}) was determined with different SRHA dosages (1.0, 3.0, and 10.0 mg L^{-1}) as a function of solution IS at pH 5.7 and 9.0. Figure 1 presents the adsorption results at pH 5.7. As seen, the adsorbed amount of SRHA to $nTiO_2$ progressively increased with increasing IS for a given initial SRHA concentration. It also increased with greater initial SRHA concentrations for a given IS. The uptake of SRHA to $nTiO_2$ ranged from 0.042 mg/m^2 at 3 mM and 1 mg L^{-1} SRHA to 0.575 mg/m^2 at 100 mM and 10 mg L^{-1} SRHA. At pH 9.0, the uptake of SRHA to $nTiO_2$ was not measurable at ISs lower than 60 mM and was very small when solution ISs increased to 60 mM or beyond for the SRHA concentrations examined (data not shown). It is well documented that HA can adsorb to metal oxide and latex particle surfaces by electrostatic interaction and specific adsorption via ligand exchange.[35,36] The results of the adsorption patterns of SRHA on $nTiO_2$ in this study are consistent with these mechanisms. As a result, the stability of the $nTiO_2$ in suspensions was dramatically enhanced in the presence of SRHA at pH 5.7, presumably due to the increased electrostatic and steric interactions between SRHA coated $nTiO_2$ particles;[37] whereas, it was hardly affected in the presence of SRHA at pH 9.0 as shown in the SI (Figure S1 and text).

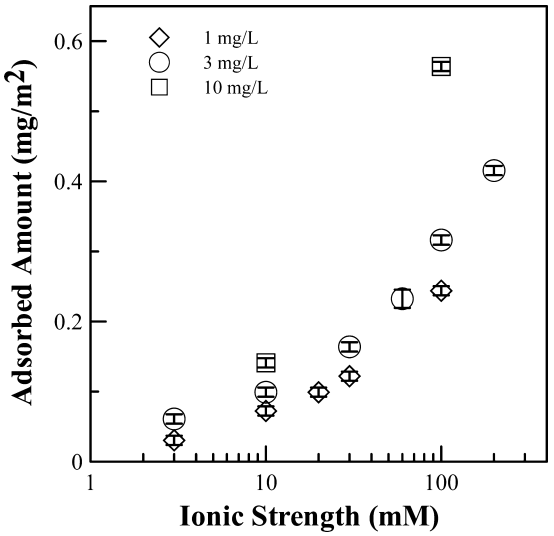

Figure 1. Adsorbed amount of SRHA on the $nTiO_2$ surface as a function of solution IS and initial SRHA concentration in the $nTiO_2$ suspensions at pH 5.7.

3.2. Electrokinetic Properties of $nTiO_2$ and Sand Surfaces. The ζ potentials of the $nTiO_2$ and the sand as a function of IS and SRHA concentration at pH 5.7 and 9.0 are presented in Figure 2. As illustrated, both the $nTiO_2$ and the sand were negatively charged over the entire range of IS and pH conditions examined. The absolute magnitude of the ζ potentials decreased with an increase in salt concentration at both pH values due to the charge screening effect and electrostatic double layer compression for all surfaces.

Interestingly, the ζ potentials of the $nTiO_2$ were not significantly different at the three SRHA concentrations (1, 3, and 10 mg L^{-1}) but there was significant difference between 0 and 1 mg L^{-1} SRHA for a given IS at pH 5.7. However, the ζ potentials of the $nTiO_2$ at pH 9.0 and the sand at the two pH levels were not affected by the presence of SRHA. No variations of ζ potentials of the $nTiO_2$ for a given IS at pH 9.0 as a function of SRHA concentrations can be explained by the low adsorption of SRHA onto the $nTiO_2$, as discussed above. Rutile surface readily develops a considerable charge density in aqueous solution at pH 9.0 through the deprotonation of its surface hydroxyl groups,[21,22] which is also suggested by the highly negative ζ potential values of $nTiO_2$ measured in this study. It is well established that SRHA molecule is highly negatively charged in aqueous solution at pH 9.0 due to the deprotonation of most of its carboxylic groups and a fraction of phenolic groups that consist of the major functional groups of SRHA molecules.[38] The low adsorption of SRHA on the $nTiO_2$

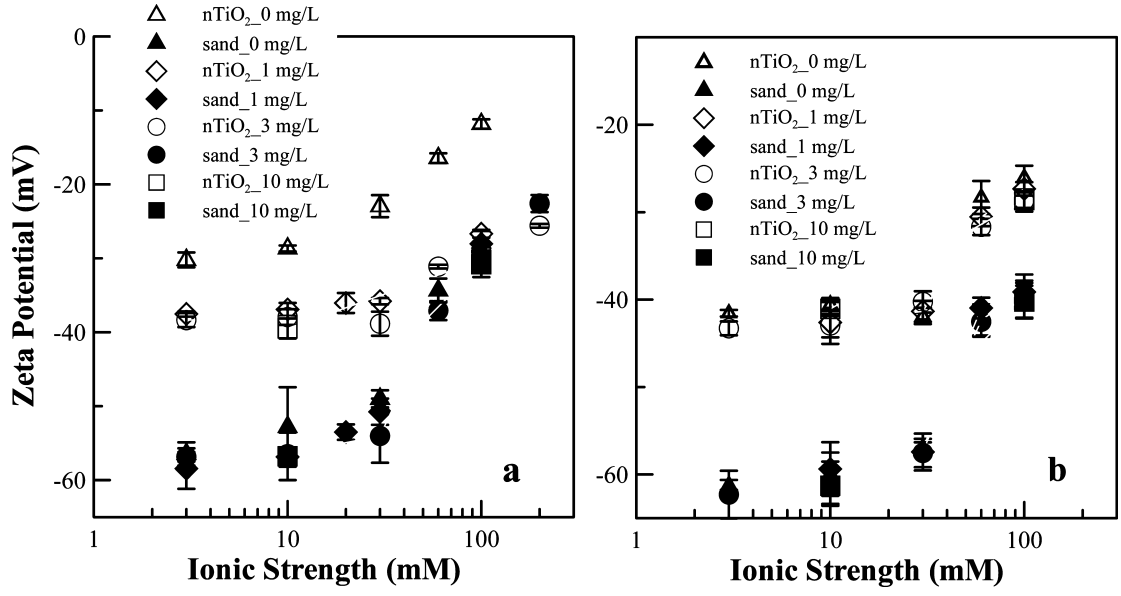

Figure 2. ζ potentials of the $nTiO_2$ and sand as a function of IS and initial SRHA concentration (in mg/L) in suspensions at (a) pH 5.7 and (b) pH 9.0. Error bars represent one standard deviation.

dx.doi.org/10.1021/es204010g | Environ. Sci. Technol. 2012, 46, 7142–7150

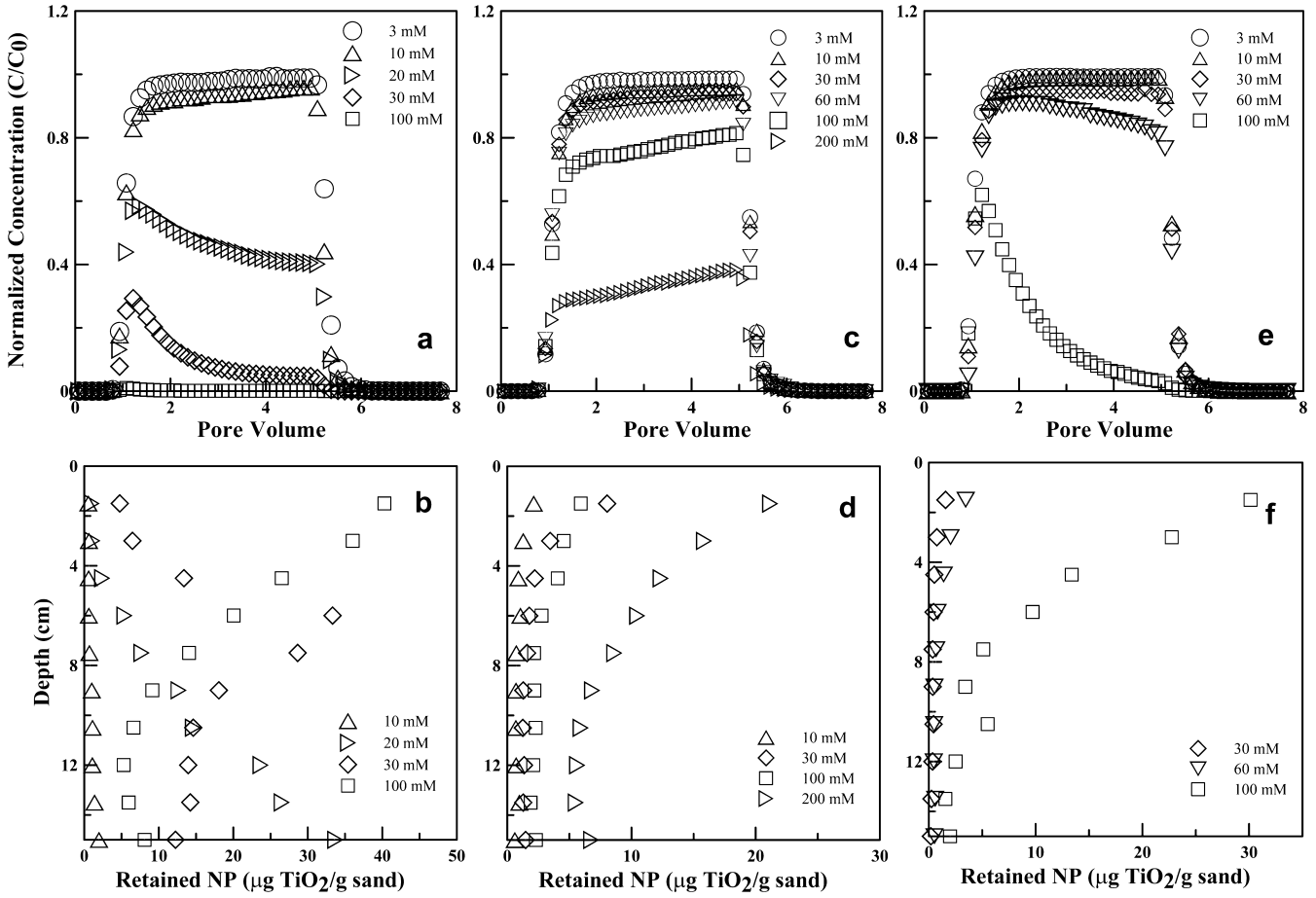

Figure 3. Representative breakthrough curves (a, c, and e) and retention profiles (b, d, and f) for the $nTiO_2$ over a wide range of solution ISs in the presence of an initial SRHA concentration of (a, b) 1 mg L^{-1}, (c, d) 3 mg L^{-1} in suspensions at pH 5.7, and (e, f) in the presence of 3 mg L^{-1} SRHA in suspensions at pH 9.0. Experimental conditions are as follows: Darcy velocity = 0.0051 cm s^{-1}, porosity = 0.37, mean sand grain diameter = 275 μm, and temperature = 22−23 °C.

as observed at pH 9.0 was most likely dominated by a strong electrostatic repulsion between SRHA molecules and the $nTiO_2$ surfaces. The same interpretation can hold in the case of sand at pH 5.7 and 9.0, which is in line with the observations previously reported.[31,36] In contrast, the adsorption of SRHA to the $nTiO_2$ resulted in more negative ζ potentials of the NPs for a given IS as compared to the values in the absence of SRHA at pH 5.7 (Figure 2). However, the ζ potential values of the SRHA coated $nTiO_2$ particles seemed to be insensitive to the different amount of adsorbed SRHA on the $nTiO_2$ at given ISs, as shown in Figure 2, similar to the observation of Domingos et al. at comparable conditions.[37]

3.3. Distinct Effects of SRHA on the Transport and Retention of $nTiO_2$ in Sand Porous Media. The $nTiO_2$ transport breakthrough curves and retention profiles were obtained for a wide range of solution chemistries, i.e., IS 3−200 mM and SRHA 0−10 mg L^{-1} at pH 5.7 and 9.0. The representative results are shown in Figures 3, S4, and S5, SI. Very similar breakthrough curves and retention profiles to those shown in Figure 3e,f were obtained for the $nTiO_2$ at the corresponding ISs in the absence and presence of SRHA of concentrations of 1 and 10 mg L^{-1} at pH 9.0 (Figure S4, SI). Compared to the transport results that the $nTiO_2$ was essentially immobile in porous media when IS was greater than 1 mM in NaCl solutions at pH 5.7 (data not shown), the mobility of the $nTiO_2$ was remarkably augmented at pH 9.0 and also in the presence of SRHA at pH 5.7, even at a SRHA concentration as low as 1 mg L^{-1}. In addition, the enhancement of the $nTiO_2$ transportability due to the presence of SRHA was limited at pH 9.0, regardless of the concentrations of SRHA examined in this study.

As seen in Figures 3 and S5, SI, when the other conditions remained the same, the normalized effluent concentrations of the $nTiO_2$ (C/C_0) were gradually reduced with increasing IS, which is consistent with the ζ potentials presented in Figure 2 that show both the $nTiO_2$ and the sand became less negatively charged with increasing IS due to the electrostatic double layer being compressed. Consequently, it resulted in an increase in the deposition rate of the $nTiO_2$ owing to the reduced electrostatic repulsive interaction. This phenomenon is in qualitative agreement with the Derjaguin−Landau−Verwey−Overbeek (DLVO) theory of colloidal stability.[39] In contrast, while the ζ potentials of the $nTiO_2$ and the sand at a given IS barely changed with varying SRHA concentrations (1−10 mg L^{-1}) at pH 5.7 (Figure 2a), more SRHA in suspensions greatly facilitated the transport of the $nTiO_2$ in sand columns, which cannot be explained in the framework of the classic DLVO theory. For instance, the $nTiO_2$ was almost completely retained in the column at 100 mM in the presence of 1 mg L^{-1} SRHA at pH 5.7 (Figure 3a), while 76% and 90% $nTiO_2$ exited from the column at 100 mM when the SRHA concentrations were increased to 3 and 10 mg L^{-1}, respectively (Figures 3c and S5

dx.doi.org/10.1021/es204010g | Environ. Sci. Technol. 2012, 46, 7142−7150

of the SI). Such effects of the presence of SRHA were not observed at pH 9.0.

The distinct effects of SRHA on the transport of the $nTiO_2$ at pH 5.7 versus pH 9.0 were further illustrated in terms of the $nTiO_2$ apparent deposition rate coefficient, k, which was experimentally determined for each condition following the procedure previously described.[40,41] Figure S6 of the SI summarizes k as a function of IS and SRHA concentration for all transport experiments. As seen, the presence of larger amounts of SRHA ($1 - 10$ mg L^{-1}) at given ISs greatly decreased the k at pH 5.7, thus increased the mobility of the $nTiO_2$ in the sand column (Figures 3 and S5, SI). The effect became more pronounced with increasing IS at pH 5.7. This enhanced mobility of the $nTiO_2$ due to the presence of greater amounts of SRHA is attributable to the larger adsorption density of SRHA to the $nTiO_2$ as discussed above. The adsorbed SRHA on the $nTiO_2$ presumably provided additional electrostatic and/or steric repulsive interactions to stabilize and mobilize the $nTiO_2$ in porous media, which will be discussed in detail later. As a result, the stability and mobility of the $nTiO_2$ at pH 5.7 was largely dependent on the aqueous concentration of SRHA. In contrast, limited influence of the presence of SRHA (0−10 mg L^{-1}) on k was observed at pH 9.0 as shown in Figure S6b, SI, which correlates well with the trend of ζ potential values in Figure 2b (i.e., no significant change of ζ potentials of the $nTiO_2$ and the sand in the absence and the presence of varying concentrations of SRHA) and the negligible adsorption of SRHA to the $nTiO_2$ as mentioned above. The transportability of the $nTiO_2$ at pH 9.0 greatly depended on the attained negative charge of the $nTiO_2$ and sand surfaces in aqueous solutions.

3.4. Mechanisms Governing the Transport and Deposition of $nTiO_2$. As shown in Figures 3 and S6, SI, the $nTiO_2$ exhibited a variety of variations with regard to its transport and retention behaviors at different solution chemistries in porous media. In order to elucidate the controlling mechanisms operating at different conditions, additional experiments and theoretical calculations were performed.

3.4.1. Possible Mechanisms Involved. As seen in Figure 3, in the presence of 1 mg L^{-1} SRHA and at pH 5.7, the breakthrough curves displayed a transition from blocking to ripening shapes (Figure 3a), and the retention profiles exhibited a gradual shift of the maximum $nTiO_2$ retention segment from the end toward the entrance of the column with increasing IS (Figure 3b). As the initial concentration of SRHA increased to 3 mg L^{-1}, the $nTiO_2$ breakthrough curves were primarily characterized as blocking in shape (Figure 3c). Meanwhile, the corresponding retention profiles showed hyper-exponential decay along the column depth (Figures 3d and S7, SI). In contrast, in the presence of 3 mg L^{-1} SRHA and at pH 9.0, the breakthrough curves showed a similar transition from blocking to ripening shapes with increasing IS (Figure 3e), while the retention profiles displayed hyper-exponential decay along the column (Figures 3f and S7, SI). It is noted that the ripening shape of the breakthrough curve and the hyper-exponential decay at 100 mM and pH 9.0 are much more pronounced.

Similar transition of the breakthrough curve shapes and a gradual shift of the maximum $nTiO_2$ retention segment along the column in the corresponding retention profiles were observed in the systems without the presence of SRHA, but at much lower IS conditions.[18] It is worth noting that the $nTiO_2$ suspensions in the presence of 1 mg L^{-1} SRHA were stable at IS no greater than 30 mM and pH 5.7 (Figure S1, SI). It is likely that SRHA coated $nTiO_2$ particles preserved certain uncoated $nTiO_2$ characteristics at these conditions due to the low SRHA adsorption density on $nTiO_2$ (Figure 1). As discussed previously,[18] the enhancement of $nTiO_2$ deposition with time (ripening, Figure 3a) were most likely attributable to more favorable interactions for deposition between approaching $nTiO_2$ and $nTiO_2$ that had been already deposited, presumably due to larger van der Waals attraction and smaller electrostatic repulsion between $nTiO_2$−$nTiO_2$ than between $nTiO_2$ and bare sand surfaces, thereby facilitating approaching $nTiO_2$ deposition onto deposited $nTiO_2$. The Hamaker constant of $nTiO_2$−water−$nTiO_2$ is greater than that of $nTiO_2$−water−silica[42] and the ζ potentials of SRHA coated $nTiO_2$ are much less negative than those of sand at the same conditions as shown in Figure 2a. Similar ripening shape breakthrough curves for $nTiO_2$ at comparable conditions were reported in the literature.[16,17] In addition, transformation of $nTiO_2$ aggregates likely occurred by collision between the $nTiO_2$ and sand grains when the $nTiO_2$ was transported in the column may explain the observed gradual shift of the maximum $nTiO_2$ retention segment along the column in retention profiles.[18] The detailed explanation on the $nTiO_2$ aggregate transformation and its impact on $nTiO_2$ transport and deposition behavior can be found in our recent study.[18] Furthermore, $nTiO_2$ aggregation and subsequent straining in porous media likely contributed to the observed $nTiO_2$ transport and retention behavior at these conditions. Similar variations in retention profiles were observed for $nTiO_2$ and other NP aggregates.[14,43]

As the concentration of SRHA in suspensions increased to 3 mg L^{-1} at pH 5.7, no such temporal and spatial variations of the $nTiO_2$ transport breakthrough curves and retention profiles were observed. It is most likely that greater SRHA adsorption on $nTiO_2$ increased the repulsive interactions between SRHA coated $nTiO_2$−$nTiO_2$ and $nTiO_2$−sand surfaces. Instead, the $nTiO_2$ deposition dynamics was characterized by the blocking of sand surfaces and declining deposition rates with increasing PVs as shown in Figure 3c, which can be explained by the limited availability of favorable sites for deposition on sand surfaces likely induced by sand surface heterogeneity.[18] Such $nTiO_2$ deposition dynamics (blocking) were not observed when IS increased to 20 mM in the presence of 1 mg L^{-1} SRHA at pH 5.7, due to the other mechanisms such as the favorable $nTiO_2$−$nTiO_2$ interactions and the transformation of $nTiO_2$ aggregates discussed above dominating the transport and deposition process of the $nTiO_2$. Furthermore, hyper-exponential profiles of the retained $nTiO_2$ were observed at these conditions (3 mg L^{-1} SRHA at pH 5.7) as presented in Figures 3d and S7, SI. It is common to observe hyper-exponential type colloid retention profiles under unfavorable deposition conditions. It is demonstrated that particle heterogeneity[44] and the concurrent existence of both favorable and unfavorable particle interactions[45] can drive hyper-exponential type retention profiles, which were likely present in our system.

Figure 3e showed a similar transition of the $nTiO_2$ transport breakthrough curve shapes to Figure 3a. However, the ripening process was substantially pronounced at 100 mM, 3 mg L^{-1} SRHA and pH 9.0 compared to those in Figure 3a. In addition, considerably different corresponding retention profiles were observed as presented in Figure 3f. The influent concentration drop of $nTiO_2$ and the mechanism of straining are likely

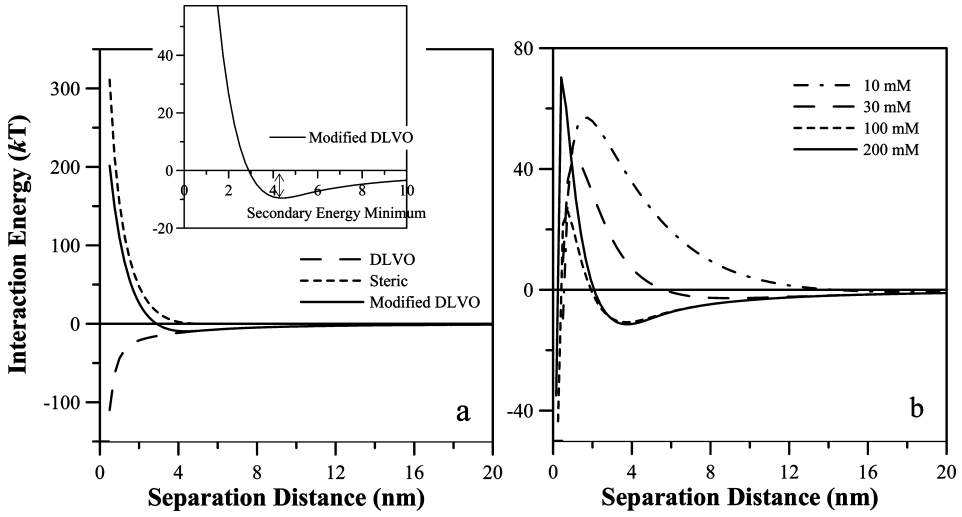

Figure 4. (a) Representative modified DLVO interaction energy calculations showing the classic DLVO interaction energy profile, the steric interaction energy profile, and the modified (total) DLVO interaction energy profile between the SRHA coated $nTiO_2$ and sand surfaces at the condition of 100 mM NaCl, 10 mg L^{-1} SRHA, and pH 5.7. (b) Calculated modified DLVO interaction energy profiles as a function of IS at conditions of 3 mg L^{-1} SRHA and pH 5.7. Interaction energies were calculated by use of the ζ potentials presented in Figure 2. A Hamaker constant of 4.5×10^{-20} J was assumed for the interacting system of $nTiO_2$–water–sand. The SRHA thickness covered on the $nTiO_2$ surface was estimated to be 5.7 nm in the calculations. The inset presents a close-up of the secondary energy minimum region of the modified DLVO interaction energy profile.

responsible for these differences and will be discussed in detail as follows. Physical straining occurs as colloidal particles are trapped in the pore throats that are too small to allow particle passage[46] and often leads to physical pore structure clogging and extensive particle accumulation near the column entrance.[47] Empirically, straining has been found to be an important particle retention mechanism when the critical diameter ratio of particles to median sand grains is greater than 0.0017.[46] Since the sand used in this study has a size of 275 μm, the critical NP aggregate size would need to be about 460 nm for straining. Considering the wide size distribution of the $nTiO_2$ particles in suspensions, hydrodynamic diameter measurements shown in Figure S1c (SI) indicated that $nTiO_2$ particles reached this critical size in 60 mM and were much bigger in 100 mM, respectively. To provide experimental evidence of straining, an additional experiment with coarse sand of an average diameter of 725 μm was conducted in the absence of SRHA and at 60 mM and pH 9.0. The comparison of the $nTiO_2$ transport breakthrough curves between the coarse and the fine sand is presented in Figure S8 (SI). As seen, it is evident that the ripening process with coarse sand was substantially less significant compared to that for the fine sand, as the $nTiO_2$ particle size was much smaller than the critical size of 1200 nm for straining in the coarse sand porous media. Moreover, the retention profiles in Figure 3f provided additional evidence for straining. Therefore, straining was an important mechanism for $nTiO_2$ retention in porous media at relatively high IS when $nTiO_2$ particles were not stable, evolved to bigger NP aggregates, and eventually physically clogged pores in porous media. Similar phenomena have been reported for iron-based NP transport in porous media.[48] It is worth noting that straining does not necessarily lead to ripening. It is likely that the enhanced $nTiO_2$ deposition in fine sand porous media due to the additional straining and greater $nTiO_2$ mass transfer to sand surfaces further promoted $nTiO_2$ straining with time, which resulted in ripening-shape breakthrough curves as seen in Figures 3e and S8, SI.

3.4.2. Modified DLVO Interaction-Energy Calculations. In order to better understand the distinct impacts of SRHA on the transport and deposition behavior of the $nTiO_2$ in porous media at various conditions, the interaction energy between the $nTiO_2$ and sand surfaces is calculated for each condition. Due to the apparent insufficiency of the conventional DLVO theory for describing the $nTiO_2$ deposition behavior observed at conditions of pH 5.7, i.e., greater SRHA concentrations (3 and 10 mg L^{-1}) relative to the lower concentration (1 mg L^{-1}) resulted in remarkably smaller $nTiO_2$ deposition rates for IS greater than 3 mM (Figure S6a, SI), whereas SRHA at these concentrations hardly affected the ζ potential values of the $nTiO_2$ and the sand (Figure 2a), the DLVO interaction energy calculations were modified by the incorporation of a steric repulsive energy determined by the Alexander-de Gennes equations[42,49] when SRHA coated $nTiO_2$ particles approach to sand surface. The details of the interaction energy calculations are provided in the SI.

The modified DLVO interaction energy profiles for the interacting $nTiO_2$ and sand at pH 5.7 are presented in Figures 4 and S9, SI, while only classic DLVO interaction energies are calculated for the conditions at pH 9.0 (Figure S9b, SI). The calculations reveal the existence of significant repulsive energy barriers (>25 kT) for $nTiO_2$ deposition at all conditions, implying unfavorable deposition conditions.[39] As observed, the calculated energy barriers decreased with increasing IS at a given SRHA concentration and pH, except at the condition of 200 mM, 3 mg/L SRHA and pH 5.7 (Figure 4b) that the steric repulsive interaction resulted in a greater energy barrier due to the high SRHA adsorption density on the $nTiO_2$ at this condition (Figure 1). Due to the presence of the sizable energy barriers at all conditions, it was not likely that the $nTiO_2$ overcame those energy barriers and deposited in a primary energy minimum.

Previous studies suggested that the secondary energy minimum can be an important mechanism for colloid deposition in porous media.[32,35,45] As seen in Figures 4 and

dx.doi.org/10.1021/es204010g | Environ. Sci. Technol. 2012, 46, 7142–7150

S9, SI, the interaction energy profiles show the presence of secondary energy minima. The secondary energy well depth and distance are summarized in Table S2 (SI) for different conditions used in the column experiments, with the wells ranging from 0.17 up to 11.37 k_BT. When the other conditions remain the same, the secondary energy wells become deeper and closer to the sand surface with increasing IS. Such interaction energy features suggest that the $nTiO_2$ can be captured in those secondary energy wells unless they have sufficient kinetic energy to escape back into solution.[40] The kinetic energy of submicrometer particles originating from Brownian motion, on average, is around 1 k_BT.[45] Hence, the calculated values of the secondary energy minima presented in Table S2 (SI) suggest that the $nTiO_2$ can readily be retained in the secondary minimum, except at the IS of 3 mM. As seen in Figures 3 and S5, SI, the $nTiO_2$ retention behavior is in qualitative agreement with the trend of increasing depth of the secondary energy minima with increasing IS. On the basis of these observations and calculations, it was hypothesized that the secondary energy minimum was an important mechanism governing the $nTiO_2$ transport and deposition in porous media observed in this study. The hypothesis was further supported by the experimental evidence, as demonstrated in the SI (see Figure S10 and text).

Close examination of the interaction energy calculations shown in Figures 4 and S9, and Table S2 (SI) also reveals the distinct effects of SRHA on the transport of the $nTiO_2$ at pH 5.7. As discussed earlier, the adsorbed SRHA on $nTiO_2$ presumably provided additional electrostatic and/or steric repulsive interactions to mobilize the $nTiO_2$ in porous media. It was evident that the interaction energies between the SRHA coated $nTiO_2$ and sand surfaces were largely controlled by the classic DLVO interactions (i.e., van der Waals and electrostatic interactions) at conditions of IS no greater than 10 mM. In other words, the enhanced transportability of the $nTiO_2$ in the presence of SRHA was likely only attributed to the elevated electrostatic repulsive interaction between the SRHA coated $nTiO_2$ and sand surfaces at those conditions. In contrast, further increases in IS resulted in greater SRHA adsorption on $nTiO_2$ (Figure 1). As a result, steric interaction provided an additional repulsive interaction to facilitate the $nTiO_2$ transport in porous media at IS greater than 10 mM and SRHA concentration greater than 1 mg L^{-1}. An illustrative example for the condition of 100 mM, 10 mg L^{-1} SRHA, and pH 5.7 is provided in Figure 4a. As seen, no energy barrier would exist without considering the steric interaction, predicting favorable deposition conditions. On the contrary, the steric interaction generated a sizable overall interaction energy barrier to prevent the $nTiO_2$ deposition in the primary energy minimum, which was consistent with the transport experiment result presented in Figure S5 (SI). Therefore, the adsorption of SRHA to $nTiO_2$ provided both electrostatic and steric repulsive interactions to mobilize $nTiO_2$ in porous media at these conditions. In addition, at a given IS, greater adsorbed SRHA on $nTiO_2$ produced shallower secondary energy wells (Table S2, SI), and, as a result, reduced k at pH 5.7 as observed in Figure S6a (SI). It is worth mentioning that the results in Figure S6a (SI) suggested a different IS of 3 mM, above which the steric repulsive interaction started to promote the $nTiO_2$ mobility in porous media as smaller k values were obtained with increasing initial SRHA concentration at a particular IS. The discrepancy of this critical IS indicated from the interaction energy calculations and the experimental observations highlights an underestimation of the effect of the steric interaction between the SRHA coated $nTiO_2$ and sand surfaces in the interaction energy calculations. Simply estimating the thickness of the adsorbed SRHA layer on $nTiO_2$ to be 5.7 nm might represent a significant oversimplification of the conformation of the adsorbed SRHA on $nTiO_2$ at different solution conditions. Apparently, advanced knowledge on the adsorbed SRHA conformation on the $nTiO_2$ and the resulting interactions between surfaces is desired to better predict the transport and deposition behavior of the $nTiO_2$ in porous media at different conditions.

Overall, this study demonstrated the distinct effects of SRHA on the stability and mobility of the $nTiO_2$ in saturated porous media. Specifically, in acidic background solutions, SRHA is readily adsorbed to the $nTiO_2$ surfaces. As a result, the adsorbed SRHA drastically enhances the stability and mobility of the $nTiO_2$. The enhancement is largely dominated by the adsorbed SRHA altering the electrokinetic property of the $nTiO_2$ particles at low adsorption densities, thus increasing the electrostatic repulsive interactions between the coated $nTiO_2$ and sand surfaces. As the adsorbed SRHA density increases, combinations of elevated electrostatic and steric interactions provide further repulsive forces to stabilize and mobilize $nTiO_2$ in aquatic environments. A modified DLVO theory presented in this study can qualitatively interpret the general trends of the $nTiO_2$ transport and retention behavior under such conditions. It is worth noting that NOM concentrations of ground and surface waters often fall in the ranges of 0.25 to 5 and 2.5 to 50 mg L^{-1}, while it can be up to a couple of g L^{-1} for wastewaters.[50] Therefore, $nTiO_2$ can be very stable and mobile in certain acidic surface waters and wastewaters due to the abundance of NOM. However, in alkaline solutions, SRHA barely adsorbs to the $nTiO_2$ surfaces. As a result, the presence of SRHA hardly affects the transport and deposition of the $nTiO_2$ at different ISs. However, the $nTiO_2$ surface can develop considerable negative charge density in alkaline solutions, thereby facilitating the $nTiO_2$ stability and mobility at such conditions. These findings might provide a clue to understand how $nTiO_2$ particles managed to pass through the extensive full scale wastewater treatment plants and showed up in treated effluents that flowed into rivers and lakes.[5,6] In addition, the information presented herein may be useful for assessing the environmental exposure, risk, and ecological implications of $nTiO_2$ and eventually developing regulations for such nanomaterials.

■ ASSOCIATED CONTENT

Ⓢ Supporting Information

Additional text, figures, and tables. This material is available free of charge via the Internet at http://pubs.acs.org.

■ AUTHOR INFORMATION

Corresponding Author

*Phone (580) 436-8651; fax (580) 436-8703; e-mail chen.gexin@epa.gov.

Notes

The authors declare no competing financial interest.

■ ACKNOWLEDGMENTS

This research was funded by the National Nanotechnology Initiative through the U.S. Environmental Protection Agency (EPA). This article has not been subjected to an internal policy

review of the U.S. EPA. Therefore, the research results do not necessarily reflect the views of the agency or its policy. We acknowledge Stephanie Burrage for her laboratory assistance through the U.S. EPA Environmental Research Apprenticeship Program (ERAP) at the Robert S. Kerr Environmental Research Center. G.C. is thankful for the help of Dr. Bin Peng at the Southwestern College in Winfield, KS and Dr. Junqi Huang at the U.S. EPA with the Matlab code. The authors are grateful to Dr. Yusong Li at University of Nebraska-Lincoln, Dr. Sharon Walker at University of California, Riverside, and three anonymous reviewers for their constructive comments that helped improve the quality of this work.

REFERENCES

(1) Chen, X.; Mao, S. S. Titanium dioxide nanomaterials: Synthesis, properties, modifications, and applications. *Chem. Rev.* **2007**, *107* (7), 2891−2959.

(2) Guzman, K. A. D.; Finnegan, M. P.; Banfield, J. F. Influence of surface potential on aggregation and transport of titania nanoparticles. *Environ. Sci. Technol.* **2006**, *40* (24), 7688−7693.

(3) Robichaud, C. O.; Uyar, A. E.; Darby, M. R.; Zucker, L. G.; Wiesner, M. R. Estimates of upper bounds and trends in nano-TiO_2 production as a basis for exposure assessment. *Environ. Sci. Technol.* **2009**, *43* (12), 4227−4233.

(4) Brar, S. K.; Verma, M.; Tyagi, R. D.; Surampalli, R. Y. Engineered nanoparticles in wastewater and wastewater sludge—Evidence and impacts. *Waste Manage.* **2010**, *30* (3), 504−520.

(5) Westerhoff, P.; Song, G.; Hristovski, K.; Kiser, M. A. Occurrence and removal of titanium at full scale wastewater treatment plants: implications for TiO_2 nanomaterials. *J. Environ. Monitor.* **2011**, *13* (5), 1195−1203.

(6) Kiser, M. A.; Westerhoff, P.; Benn, T.; Wang, Y.; Perez-Rivera, J.; Hristovski, K. Titanium nanomaterial removal and release from wastewater treatment plants. *Environ. Sci. Technol.* **2009**, *43* (17), 6757−6763.

(7) Scown, T. M.; van Aerle, R.; Tyler, C. R. Review: Do engineered nanoparticles pose a significant threat to the aquatic environment? *Crit. Rev. Toxicol.* **2010**, *40* (7), 653−670.

(8) Zhu, X.; Zhou, J.; Cai, Z. TiO_2 nanoparticles in the marine environment: Impact on the toxicity of tributyltin to abalone (*Haliotis diversicolor supertexta*) embryos. *Environ. Sci. Technol.* **2011**, *45* (8), 3753−3758.

(9) Comarmond, M. J.; Payne, T. E.; Harrison, J. J.; Thiruvoth, S.; Wong, H. K.; Aughterson, R. D.; Lumpkin, G. R.; Muller, K.; Foerstendorf, H. Uranium sorption on various forms of titanium dioxide: Influence of surface area, surface charge, and impurities. *Environ. Sci. Technol.* **2011**, *45* (13), 5536−5542.

(10) Pena, M.; Meng, X. G.; Korfiatis, G. P.; Jing, C. Y. Adsorption mechanism of arsenic on nanocrystalline titanium dioxide. *Environ. Sci. Technol.* **2006**, *40* (4), 1257−1262.

(11) Wiesner, M. R.; Lowry, G. V.; Alvarez, P.; Dionysiou, D.; Biswas, P. Assessing the risks of manufactured nanomaterials. *Environ. Sci. Technol.* **2006**, *40* (14), 4336−4345.

(12) Lecoanet, H. F.; Wiesner, M. R. Velocity effects on fullerene and oxide nanoparticle deposition in porous media. *Environ. Sci. Technol.* **2004**, *38* (16), 4377−4382.

(13) Lecoanet, H. F.; Bottero, J. Y.; Wiesner, M. R. Laboratory assessment of the mobility of nanomaterials in porous media. *Environ. Sci. Technol.* **2004**, *38* (19), 5164−5169.

(14) Choy, C. C.; Wazne, M.; Meng, X. G. Application of an empirical transport model to simulate retention of nanocrystalline titanium dioxide in sand columns. *Chemosphere* **2008**, *71* (9), 1794−1801.

(15) Joo, S. H.; Al-Abed, S. R.; Luxton, T. Influence of carboxymethyl cellulose for the transport of titanium dioxide nanoparticles in clean silica and mineral-coated sands. *Environ. Sci. Technol.* **2009**, *43* (13), 4954−4959.

(16) Solovitch, N.; Labille, J.; Rose, J.; Chaurand, P.; Borschneck, D.; Wiesner, M. R.; Bottero, J. Y. Concurrent aggregation and deposition of TiO_2 nanoparticles in a sandy porous media. *Environ. Sci. Technol.* **2010**, *44* (13), 4897−4902.

(17) Godinez, I. G.; Darnault, C. J. G. Aggregation and transport of nano-TiO_2 in saturated porous media: Effects of pH, surfactants and flow velocity. *Water Res.* **2011**, *45* (2), 839−851.

(18) Chen, G.; Liu, X.; Su, C. Transport and retention of TiO_2 rutile nanoparticles in saturated porous media under low-ionic-strength conditions: Measurements and mechanisms. *Langmuir* **2011**, *27* (9), 5393.

(19) Ben-Moshe, T.; Dror, I.; Berkowitz, B. Transport of metal oxide nanoparticles in saturated porous media. *Chemosphere* **2010**, *81* (3), 387−393.

(20) Chowdhury, I.; Hong, Y.; Honda, R. J.; Walker, S. L. Mechanisms of TiO_2 nanoparticle transport in porous media: Role of solution chemistry, nanoparticle concentration, and flowrate. *J. Colloid Interface Sci.* **2011**, *360* (2), 548−555.

(21) Svecova, L.; Cremel, S.; Sirguey, C.; Simonnot, M. O.; Sardin, M.; Dossot, M.; Mercier-Bion, F. Comparison between batch and column experiments to determine the surface charge properties of rutile TiO_2 powder. *J. Colloid Interface Sci.* **2008**, *325* (2), 363−370.

(22) Yates, D. E.; Healy, T. W. Titanium dioxide electrolyte interface. 2. Surface-charge (titration) studies. *J. Chem. Soc. Faraday Trans. I* **1980**, *76*, 9−18.

(23) Aiken, G. R.; Hsu-Kim, H.; Ryan, J. N. Influence of dissolved organic matter on the environmental fate of metals, nanoparticles, and colloids. *Environ. Sci. Technol.* **2011**, *45*, 3196−3201.

(24) Johnson, R. L.; Johnson, G. O.; Nurmi, J. T.; Tratnyek, P. G. Natural organic matter enhanced mobility of nano zerovalent iron. *Environ. Sci. Technol.* **2009**, *43* (14), 5455−5460.

(25) Espinasse, B.; Hotze, E. M.; Wiesner, M. R. Transport and retention of colloidal aggregates of C_{60} in porous media: Effects of organic macromolecules, ionic composition, and preparation method. *Environ. Sci. Technol.* **2007**, *41* (21), 7396−7402.

(26) Chen, K. L.; Elimelech, M. Interaction of fullerene (C_{60}) nanoparticles with humic acid and alginate coated silica surfaces: Measurements, mechanisms, and environmental implications. *Environ. Sci. Technol.* **2008**, *42* (20), 7607−7614.

(27) Wang, P.; Shi, Q. H.; Liang, H. J.; Steuerman, D. W.; Stucky, G. D.; Keller, A. A. Enhanced environmental mobility of carbon nanotubes in the presence of humic acid and their removal from aqueous solution. *Small* **2008**, *4* (12), 2166−2170.

(28) Jiang, X. J.; Tong, M. P.; Li, H. Y.; Yang, K. Deposition kinetics of zinc oxide nanoparticles on natural organic matter coated silica surfaces. *J. Colloid Interface Sci.* **2011**, *350* (2), 427−434.

(29) Kretzschmar, R.; Borkovec, M.; Grolimund, D.; Elimelech, M. Mobile subsurface colloids and their role in contaminant transport. *Adv. Agron.* **1999**, *66*, 121−193.

(30) Kretzschmar, R.; Sticher, H. Transport of humic-coated iron oxide colloids in a sandy soil: Influence of Ca^{2+} and trace metals. *Environ. Sci. Technol.* **1997**, *31* (12), 3497−3504.

(31) Amirbahman, A.; Olson, T. M. Transport of humic matter-coated hematite in packed beds. *Environ. Sci. Technol.* **1993**, *27* (13), 2807−2813.

(32) Hahn, M. W.; O'Melia, C. R. Deposition and reentrainment of Brownian particles in porous media under unfavorable chemical conditions: Some concepts and applications. *Environ. Sci. Technol.* **2004**, *38* (1), 210−220.

(33) Liu, X.; Chen, G.; Su, C. Effects of material properties on sedimentation and aggregation of titanium dioxide nanoparticles of anatase and rutile in the aqueous phase. *J. Colloid Interface Sci.* **2011**, *363* (1), 84−91.

(34) Aiken, G. R.; Brown, P. A.; Noyes, T. L.; Pinckney, D. J. In *Humic Substances in the Suwannee River, Georgia: Interaction, Properties, and Proposed Structures*; Averett, R. C., Ed.; U.S. Geological Survey Water Supply Paper 2372; U.S. Government Printing Office: Washington, DC, 1994.

(35) Franchi, A.; O'Melia, C. R. Effects of natural organic matter and solution chemistry on the deposition and reentrainment of colloids in porous media. *Environ. Sci. Technol.* **2003**, *37* (6), 1122−1129.
(36) Yang, K.; Lin, D. H.; Xing, B. S. Interactions of humic acid with nanosized inorganic oxides. *Langmuir* **2009**, *25* (6), 3571−3576.
(37) Domingos, R. F.; Tufenkji, N.; Wilkinson, K. J. Aggregation of titanium dioxide nanoparticles: Role of a fulvic acid. *Environ. Sci. Technol.* **2009**, *43* (5), 1282−1286.
(38) Duval, J. F. L.; Wilkinson, K. J.; van Leeuwen, H. P.; Buffle, J. Humic substances are soft and permeable: Evidence from their electrophoretic mobilities. *Environ. Sci. Technol.* **2005**, *39* (17), 6435−6445.
(39) Elimelech, M., Gregory, J., Jia, X., Williams, R. A. *Particle Deposition and Aggregation: Measurement, Modeling and Simulation*; Butterworth-Heinemann: Woburn, MA, 1995; p 441.
(40) Walker, S. L.; Redman, J. A.; Elimelech, M. Role of cell surface lipopolysaccharides in *Escherichia coli* K12 adhesion and transport. *Langmuir* **2004**, *20* (18), 7736−7746.
(41) Tufenkji, N.; Elimelech, M. Correlation equation for predicting single-collector efficiency in physicochemical filtration in saturated porous media. *Environ. Sci. Technol.* **2004**, *38* (2), 529−536.
(42) Petosa, A. R.; Jaisi, D. P.; Quevedo, I. R.; Elimelech, M.; Tufenkji, N. Aggregation and deposition of engineered nanomaterials in aquatic environments: Role of physicochemical interactions. *Environ. Sci. Technol.* **2010**, *44* (17), 6532−6549.
(43) Li, Y. S.; Wang, Y. G.; Pennell, K. D.; Abriola, L. M. Investigation of the transport and deposition of fullerene (C_{60}) nanoparticles in quartz sands under varying flow conditions. *Environ. Sci. Technol.* **2008**, *42* (19), 7174−7180.
(44) Tong, M. P.; Johnson, W. P. Colloid population heterogeneity drives hyperexponential deviation from classic filtration theory. *Environ. Sci. Technol.* **2007**, *41* (2), 493−499.
(45) Tufenkji, N.; Elimelech, M. Deviation from the classical colloid filtration theory in the presence of repulsive DLVO interactions. *Langmuir* **2004**, *20* (25), 10818−10828.
(46) Bradford, S. A.; Yates, S. R.; Bettahar, M.; Simunek, J., Physical factors affecting the transport and fate of colloids in saturated porous media. *Water Resour. Res.* **2002**, *38*, (12).
(47) Wang, Y. G.; Li, Y. S.; Kim, H.; Walker, S. L.; Abriola, L. M.; Pennell, K. D. Transport and retention of fullerene nanoparticles in natural soils. *J. Environ. Qual.* **2010**, *39* (6), 1925−1933.
(48) Hong, Y. S.; Honda, R. J.; Myung, N. V.; Walker, S. L. Transport of iron-based nanoparticles: Role of magnetic properties. *Environ. Sci. Technol.* **2009**, *43* (23), 8834−8839.
(49) Byrd, T. L.; Walz, J. Y. Interaction force profiles between *Cryptosporidium parvum* Oocysts and silica surfaces. *Environ. Sci. Technol.* **2005**, *39* (24), 9574−9582.
(50) Crittenden, J. C.; Trussell, R. R.; Hand, D. W.; Howe, K. J.; Tchobanoglous, G. *Water Treatment: Principles and Design*, 2nd ed.; John Wiley & Sons, Inc.: New York, 2005; p 1948.